Pt particle size affects both the charge separation and water reduction efficiencies of CdS-Pt nanorod photocatalysts for light-driven H_2 generation

Yawei Liu[1], Wenxing Yang[1,2]*, Qiaoli Chen[1,3,4], David A. Cullen[5], and Zhaoxiong Xie[3], Tianquan Lian[1]*

[1]Department of Chemistry, Emory University, 1515 Dickey Drive, NE, Atlanta, Georgia 30322, United States

[2]Center of Artificial Photosynthesis for Solar Fuels, School of Science, Westlake University, Hangzhou, 18 Shilongshan Road, Hangzhou 310024, Zhejiang Province, China

[3]State Key Laboratory for Physical Chemistry of Solid Surfaces and Department of Chemistry, College of Chemistry and Chemical Engineering, Xiamen University, Xiamen 361005, China;

[4]State of Laboratory Breeding Base of Green Chemistry Synthesis Technology and College of Chemical Engineering, Zhejiang University of Technology, Hangzhou 310014, China

[5]Center for Nanophase Materials Sciences, Oak Ridge National Laboratory, Oak Ridge, TN 37831, USA

Corresponding author emails:

yangwenxing@westlake.edu.cn

tlian@emory.edu

Abstract

Decreasing the metal catalyst size into nanoclusters or even single atom is an emerging direction of developing more efficient and cost-effective photocatalytic systems. Because the catalyst particle size affects both the catalyst activity and light driven charge separation efficiency, their effects on the overall photocatalytic efficiency is still poorly understood. Herein, using a well-defined semiconductor-metal heterostructure with Pt nanoparticle catalysts selectively grown on the apexes of CdS nanorods (NRs), we study the effect of the Pt catalyst size on light driven H_2 generation quantum efficiency (QE_{H_2}). With the increase of the Pt catalyst size from 0.7±0.3 to 3.0±0.8 nm, the QE_{H_2} of CdS-Pt increases from 0.5±0.2% to 38.3±5.1%, by nearly two orders of magnitude. Transient absorption spectroscopy

measurement reveals that the electron transfer rate from the CdS NR to the Pt tip increase with the Pt diameter following a scaling law of $d^{5.6}$, giving rise to the increase of electron transfer efficiency at larger Pt sizes. The observed trend can be understood by a simplified kinetic model that assumes the overall efficiency is the product of the quantum efficiencies of charge separation (including hole transfer, electron transfer and hole scavenging) and water reduction steps, and for CdS-Pt NRs, the quantum efficiencies of electron transfer and water reduction steps increase with the Pt sizes. Our findings suggest the importance of improving the quantum efficiencies of both charge separation and catalysis in designing efficient semiconductor-metal hybrid photocatalysts, especially in the regime of small metal particle sizes.

Keywords: photocatalysis, artificial photosynthesis, electron transfer, H_2 production, water reduction, nanorods, nanorod heterostructures

Introduction

Artificial photosynthesis has attracted enormous research interests in the past decades due to its promise as a renewable energy resource for a sustainable society.[1-5] Among various reported approaches, heterogenous hybrid photocatalysts composed of semiconductor/metal nanoparticle heterostructures are particularly attractive because they combine both the superior light-harvesting of semiconductors and the catalytic properties of metal catalysts.[4-11] The size of catalysts is one of the most important parameters in the design of these systems, because it can significantly affect not only the catalytic activity and selectivity, but also the cost of these systems, especially for precious noble metal catalysts.[12-13] The size dependent catalytic properties of noble metal nanoparticles have been extensively studied under electro- or thermal-catalytic conditions, in the absence of light.[14-19] However, it is unclear to what extent the insight obtained in these dark conditions can be used to guide the design of photocatalysts composed of semiconductor/metal heterostructures. The overall performance of the hybrid photocatalyst depends on the light harvesting properties of the semiconductor domain, charge separation and recombination across the semiconductor/metal interface, and the catalytic activities of the metal nanoparticle.[20-21] The size of the metal catalyst may have complex effects on all these aspects,

especially at the subnanometer regime where the density of states changes rapidly with size.

The photocatalytic performance of semiconductor/metal hybrid catalysts have been reported to depend on the metal domain size. Many of these studies focus on Pt, one of the most efficient catalysts for water splitting and H_2 evolution,[14-15, 18, 22-23] with significant effort devoted to reducing the Pt catalyst size from large particles of several nm,[24-25] to small clusters of tens of atoms,[20, 26-28]and, more recently, to the single atom level.[14-15, 29-31] Despite these efforts, mechanistic understanding of the effect of the metal catalyst size remains elusive due in part to the difficulty in designing material systems in which the metal particle number density and sizes can be systematically tuned without affecting the semiconductor or support domain.[20, 26] The recent development of semiconductor-metal hybrid nanorod heterostructures offers unique opportunities to study the size effects of metal catalysts in photocatalysts.[32-35] These structures consist of semiconductor NRs with 1 or 2 metal nanoparticles selectively deposited at the NR tips; and the size of the metal tip can be independently and systematically tuned without changing the NR domain.[32, 34] Using this materials platform, CdS NRs decorated with Au and Ni nanoparticles have been examined to understand the effect of metal particle sizes on their photocatalytic H_2 generation performances.[36-38] These studies are focused on particle diameters from ~ 2 – 10 nm and did not extend into the subnanometer size regime. Furthermore, although Pt is one of the most widely studied and CdS-Pt NRs and nanoplatelets are among the best performing photocatalysts for H_2 generation,[29, 39-41] systematic study of the effect of Pt size on their photocatalytic performance has not been reported.

Here, we utilize CdS-Pt NR heterostructures as a platform to investigate the effect of Pt size on the photocatalytic light-to-H_2 conversion efficiency in small Pt size regimes, from 0.7±0.3 to 3.0±0.8 nm. We first measured the overall light to H_2 conversion efficiencies as a function of Pt particle size under steady-state light illumination. To gain insight into the key efficiency limiting steps, we carried out *in situ* transient absorption (TA) spectroscopic measurement of charge separation and recombination kinetics of these nanorods. We propose a simplified model that divides the overall process into charge separation and water reduction stages, and using this model, the size dependence of overall light-to-H_2 conversion can be understood by the increase of both the charge separation and water reduction quantum efficiencies at larger Pt sizes. Finally, our analysis suggests that the electron transfer (ET) rate

from the CdS to Pt with size smaller than 1 nm is extreme slow. Increasing Pt size facilitates the ET due to the increase of the electronic coupling strength and density of accepting states. Our findings provide important insight into designing semiconductor-metal hybrid photocatalysts with small metal particle sizes.

Results

CdS NR Characterization

The 1D CdS and CdS-Pt NRs were synthesized according to previous literature procedures with slight modifications (SI1).[32, 42] Transmission electron microscope (TEM) measurements (Figure 1A) show that the length and diameter of CdS NRs are 26.8±3.1 and 3.7±0.4 nm, respectively. Starting from the same batch of CdS NRs, five CdS-Pt NR samples with average Pt tip diameters of 0.7±0.3, 1.4±0.8, 2.3±1.1, 2.5±1.0, and 3.0±0.8 nm were prepared. Their TEM images are shown in Figure 1B-F and the histograms of Pt size distributions are shown in Figure S1 and Table S1. These CdS-Pt NR samples show broad Pt size distributions from 0.5 to 5 nm with the relative weight of the subpopulations shifting with the average size. Thus, the observed different average performance of samples to be discussed below reflects different relative contributions of the subpopulations of Pt sizes. To avoid confusion, in the following text, we use the "average Pt size" to refer to the average H_2 production and kinetics of different samples, and we use "Pt size" when a more precise size range is referred, such as in discussion of the size-dependent ET rates. The distributions of the number of Pt tips on the NR are also listed in Table S2. Those samples can be regarded as mainly singly-tipped samples, while the $CdSPt_{3.0nm}$ sample shows a larger double-tip percentage. Previous studies have shown that when the Pt precursor/ NR ratio is low, the Pt is mainly deposited on the S-rich end.[34] However, due to a higher loading of Pt precursor in $CdSPt_{3.0nm}$, Pt tips are unavoidably deposited at both ends. All CdS and CdS-Pt NR samples with native phosphonate ligands are ligand-exchanged with 11-mercaptoundecanoic acid (MUA) into aqueous solutions by standard methods (See SI1), unless otherwise noted. UV-vis absorption spectra of both CdS and CdS-Pt NRs in water show clear exciton bands with the lowest energy 1Σ exciton band at ~460 nm (Figure 1G), determined by quantum confinement in the NR radial direction.[43-44] In comparison, the CdS-Pt NR shows

an additional broad absorption feature extending from the near IR into visible region, consistent with the Pt d-sp interband transition.[45] The absorption spectra of all five CdS-Pt NR samples are well described by the linear combination of the CdS NR and Pt particle absorption features (black dashed lines in Figure 1G), indicating that the deposition of Pt has little impact on the electronic transitions of CdS NRs.

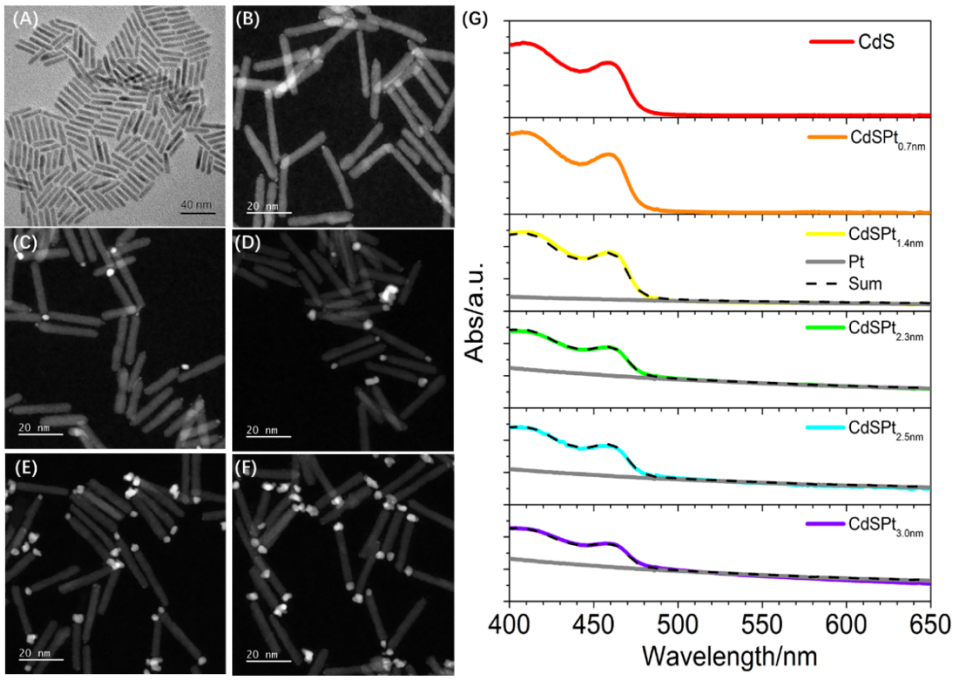

Figure 1. TEM images and absorption spectra of CdS and CdS-Pt NRs. (A-F) TEM images of (A) CdS, (B) $CdSPt_{0.7nm}$, (C) $CdSPt_{1.4nm}$, (D) $CdSPt_{2.3nm}$, (E) $CdSPt_{2.5nm}$, and (F) $CdSPt_{3.0nm}$. (G) UV-vis absorption spectra of CdS and CdS-Pt NRs (colored solid lines). Also shown are fits to the CdS-Pt spectra (black dashed lines) by the linear combination of the absorption spectra of isolated Pt particles (grey solid lines) and CdS NRs. This indicates the deposition of Pt has little impact on the CdS exciton bands.

Size-dependent H_2 Production Performance

The size-dependent H_2 production performance of 11-MUA capped CdS-Pt NRs dispersed in water was measured under 405 nm LED illumination (~100 mW/cm^2) for approximately 1 hour. The solution ODs of all samples were controlled to be around 0.4 at 405 nm in 1 cm pathlength cuvette; 3 mg/mL L-cysteine was added as the sacrificial donor (SD)[46]; Solution pH was tuned to 12 by adding KOH, because measurements using similar CdS-Pt NRs from pH 7 to 14 shows the highest QE_{H_2} at this pH (Figure S2). The optimal pH value for H_2 generation in this system differs from previous reports of related systems that uses alcohol as

the SD, likely due to difference in the SD.[39, 47-48] Thiols, such as 3-mercaptopropionic acid (MPA),[49-51] 11-MUA,[51] L-cysteine[46, 52] have been widely used as SDs in photocatalysis and have been shown to effectively trap the hole in CdS and lead to reduced photoluminescence of colloidal nanocrystals.[39, 51] Hole transfer to thiol containing SD molecules in the solution generates R-S$^{\cdot}$ radicals; and two oxidized radicals can further undergo irreversible bonding to form a disulfide molecule with negligible other biproducts.[46, 53] In our study, the amount of generated H_2 was quantified by gas chromatography and 3 samplings were taken every 20-30 mins during the measurement. As shown in Figure 2B, the detected H_2 amount increases linearly with the illumination time, indicative of stable H_2 production rates, and the H_2 generation rates increase with the average Pt size. The internal quantum efficiency is defined as $QE_{H_2} = \frac{2k_{H2}}{k_{photon}} * 100\%$, where k_{H_2} is the H_2 production rate, represented by the slope of the linear fit in Figure 2B, and k_{photon} is the photon absorption rate by CdS NRs at 405 nm, which is the product of photon flux and absorption of CdS NRs. This QE excludes any performance differences due to the variation of light absorption by different NR samples. The measured QE_{H_2}values of pristine CdS NRs and CdS-Pt NR without L-cysteine are <0.1%, close to our detection limit (Figure S3). Under the same experimental conditions, much higher QE_{H_2} are observed in CdS-Pt NRs with the presence of SDs, indicating the importance of Pt catalysts and SDs for H_2 production (Figure 2C, violet circles). With an increase of average Pt catalyst size from 0.7±0.3 to 3.0±0.8 nm, the $QE_{H_2}$of CdS-Pt increases from 0.5±0.2% to 38.3±5.1%, by nearly two orders of magnitude.

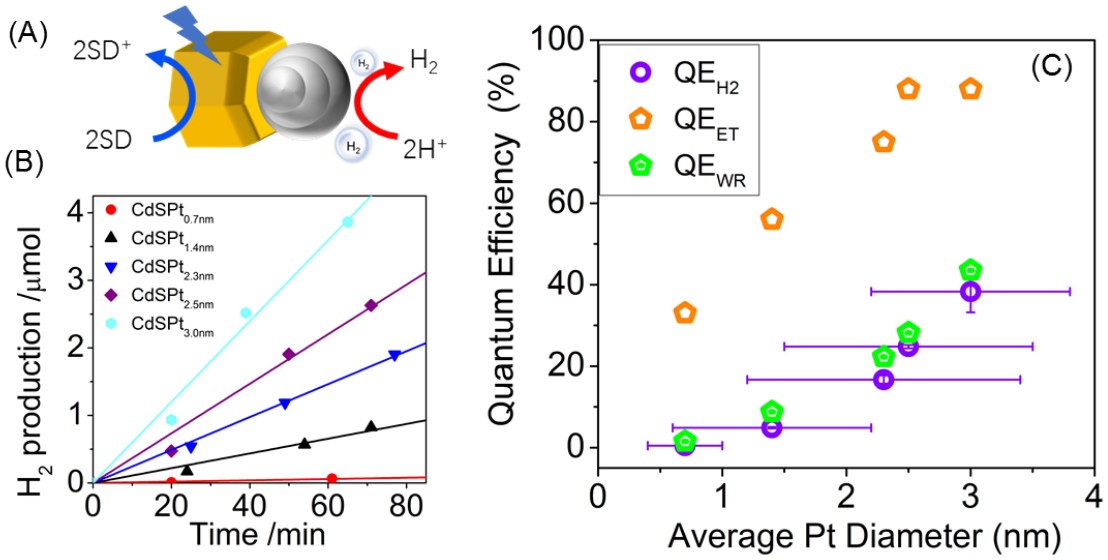

Figure 2. Photo-driven H_2 generation using CdS-Pt NRs. (A) Schematic of overall light driven H_2 generation: the overall process of forming one H_2 involves the absorption of two photons by CdS, the reduction of two H^+ on the Pt nanoparticle, and oxidation of two sacrificial donors (SD, L-cysteine) in solution. (B) The amount of light driven H_2 production as a function of illumination time for CdSPt NR samples of different average Pt tip sizes. (C) Photo-driven H_2 production internal quantum efficiency QE_{H_2} of CdS-Pt NRs as a function of the average Pt tip size. Measurement conditions: 405nm LED illumination at ~100 mW/cm^2, pH=12, 3 mg/mL L-cysteine as SDs**.** Also shown is the ET quantum efficiency QE_{ET} determined from transient absorption kinetics and the water reduction quantum efficiency $C * QE_{WR}$ calculated by the ratio of QE_{H_2} and QE_{ET} according to Eq. (1).

Charge separation and recombination kinetics

The overall light-to-H_2 conversion processes involves many competing elementary steps. To gain further insight, we utilized TA spectroscopy to directly measure the size dependence of ET kinetics from the CdS NR to Pt tip, following previous reports.[39, 42, 51] TA studies of CdS and CdS-Pt NRs were conducted with 400 nm pulse laser photoexcitation at a fluence of ~2 mW/cm^2. Under this condition, the average exciton number per NR is estimated to be ~0.1-0.2 following previously reported methods, and the measured transient signal is dominated by NRs with one exciton.[54-56] The measurements were conducted under conditions (solution pH and

sacrificial donor concentration) that are the same as the H_2 generation efficiency measurement described above (SI3), with the exception that the CW LED illumination at 405nm is replaced by pulse laser excitation at 400 nm. The same electrolyte environment is important when making a direct comparison between the photoinduced charge transfer results and photocatalytic performances because the charge transfer rates of photocatalysts depend strongly on the electrolyte environments.[57-58] The TA spectra of CdS NRs (Figure 3A) show two major features: (a) a bleach of 1Σ exciton band (XB) centered at 460 nm due to the electron filling at the conduction band (CB) edge which reduces 1Σ exciton absorption in excited NRs and (b) an photoinduced exciton absorption (XA) at ~425 nm that is attributed to red-shift of a higher energy transitions in excited NRs.[42] Because the XB bleach reflects only the populations of photogenerated CB edge electrons in the CdS NR, its decay probes the recombination of photogenerated electrons with the holes in the NR and/or ET from the NR to Pt. As shown in Figure 3D, for bare CdS NRs, the XB decay can be fit to a stretched exponential decay $\Delta A(t) = e^{-(t/\tau_x)^{\beta}}$, with the time constant τ_x and β of 17±1 ns and 0.40±0.01, respectively, which corresponds to an averaged lifetime of 57±2 ns. This highly non-single-exponential XB decay in bare CdS NRs has been attributed to the recombination of the CB electron with the trapped hole.[42] The TA spectra of selected CdS-Pt NRs, regardless of the average Pt size, show similar spectral features as those in CdS NRs, as shown in Figure 3B and C for $CdSPt_{0.7nm}$ and $CdSPt_{3.0nm}$, respectively, and in Figure S4 for other samples. However, the XB and XA features decay on a much faster time scale, which is attributed to ET from the CdS CB edge to the Pt tip. With increasing average Pt size from 0.7±0.3 nm to 3.0±0.8 nm (Figure 3D), the XB half lifetimes reduces progressively from 2.2±0.2 ns to only 8±1 ps, indicating a faster ET from the CdS NR to Pt tip at larger average Pt tip size (Table S3).

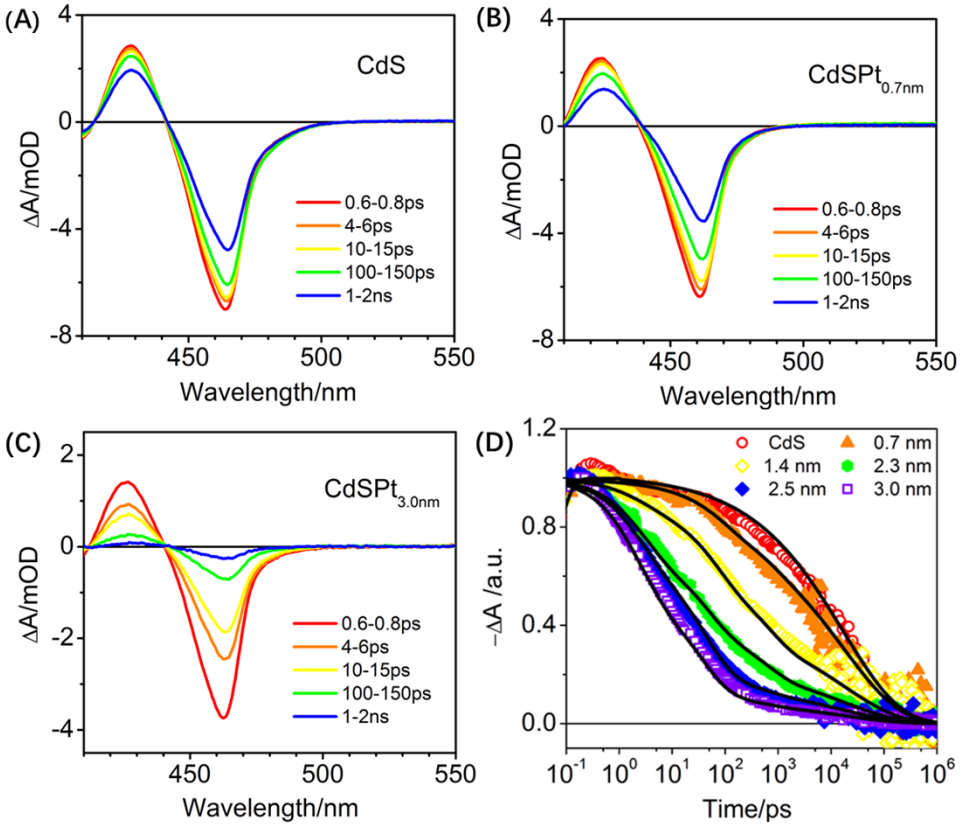

Figure 3. Transient absorption spectra and kinetics of CdS and CdS-Pt NRs. Transient absorption spectral evolution of CdS (A), CdS-$Pt_{0.7nm}$ (B), and CdS-$Pt_{3.0nm}$ (C) at indicated delay times after 400 nm excitation. For clarity, only averaged spectra in selected time delay windows are plotted. (D) Comparison of the normalized 1Σ exciton bleach recovery kinetics of CdS and 5 CdS-Pt samples (colored symbols) and their fits (solid lines) to a model described in SI4. Faster bleach recovery at larger average Pt sizes is attributed to increased ET rates.

Previous studies have shown that in the charge separated state, the presence of holes in the nanorod shifts the exciton transition energy and leads to a derivative like TA feature that can be used to follow the lifetime of charge separated state.[42, 51] Interestingly, with MUA ligand capped CdS-Pt NRs under light driven H_2 conditions described above, such charge separated state signal was not observed (Figure S5), which likely indicates a fast transfer of the hole to excess L-cysteine molecules in the solution or large dielectric screening by water. To probe the size dependent charge recombination rate, we carried out TA study of CdS-Pt NRs capped with phosphonates in toluene. The transient spectra of phosphonate capped $CdSPt_{2.5nm}$ from 10 ns to 100 μs are compared in Figure S6, which shows characteristic derivative like features of the

charge separated state. A comparison of decay kinetics of this charge separated state signal for phosphonate-capped $CdSPt_{1.4nm}$, $CdSPt_{2.3nm}$ $CdSPt_{2.5nm}$ in toluene (Figure S7) shows that the charge recombination kinetics are independent of the average Pt size with a half lifetime of ~2.3 μs. Previous studies have shown that the charge recombination is limited by the activation of holes to the valence band (VB) from hole acceptors, which may explain the slow Pt-size independent recombination kinetics.[59] Under the H_2 evolution conditions in water, the trapped holes are rapidly transferred to surface ligand MUA, which likely further slowing down the charge recombination process.

Discussion

Size-dependent efficiencies of charge separation and water reduction

The overall light-driven H_2 generation process in CdS-Pt NRs reduces two protons or water to H_2 and oxidizes two L-cysteine molecules, with energy provided by the absorption of two photons. This overall process involves multiple competing elementary steps, including charge transfer, recombination and catalysis. The key steps and intermediates are shown in Scheme 1A.[36, 51] Although we cannot differentiate whether proton or water reduction is the main pathway, the latter likely dominates at our experimental conditions of pH12. For simplicity only the proton reduction pathway is depicted in the scheme below, but all discussions below are applicable to both pathways. Scheme 1A also shows the redox potentials, relative to the reversible hydrogen electrode (RHE), of key components in this photocatalytic system at pH 12: the CdS CB (-0.3 V) and VB (+2.3 V) edges positions, the oxidation potentials of MUA (denoted as L, +1.1 V) and L-cysteine (denoted as SD, +0.6~+0.8 V), and the proton or water reduction potential (0 V). The Pt Fermil level is assumed to be equilibrated with the water reduction potential prior to light illumination. The details of estimating these redox potentials and the references can be found in SI2.3. Due to distinctly different time scales for different steps, the overall H_2 production can be divided into four stages: hole transfer from CdS to surface ligands, electron transfer from CdS to Pt, hole removal by SD and water reduction. In each stage, the forward charge transfer process competes with backward charge recombination, as detailed below.

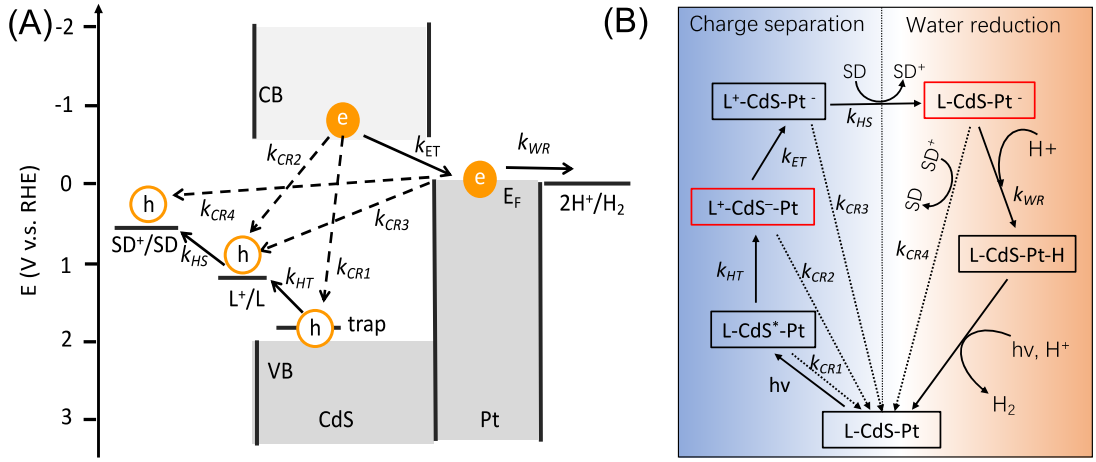

Scheme 1. (A) Key energy levels and elementary processes and (B) simplified kinetic model with key intermediate states and processes for light driven H_2 generation using L-CdS-Pt nanorods. L indicates the MUA capping ligands on the CdS surface. Forward processes (solid arrows): hole transfer from the trapped exciton state to surface ligand L (with a rate constant k_{HT}), electron transfer from the CdS to Pt (k_{ET}), hole transfer from the oxidized surface ligand L^+ to sacrificial donor SD (k_{HS}), water reduction on reduced Pt particle (k_{WR}). Each process competes with a charge recombination process (k_{CRi}, i=1-4, dashed arrows), which determines their quantum efficiency. The overall quantum efficiency of light drive H_2 generation is the product of the quantum efficiencies of the elementary steps.

The photoexcitation of MUA-capped CdS-Pt NRs, denoted as L-CdS-Pt, generates an exciton in the CdS NR. The VB hole is transferred to a trap state (likely the S dangling bond) on a sub-picosecond time scale to form a trapped exciton in CdS (L-CdS*-Pt).[42, 60] The trapped hole in L-CdS*-Pt is transferred to the MUA ligand with a rate constant k_{HT} of ~(100 ps)$^{-1}$ to form L^+-CdS—Pt according to previous reports of similar CdS-Pt NRs; [39, 51] and the hole transfer QE (QE_{HT}) is determined by its competition with the electron-hole recombination process within CdS* (k_{CR1}). The latter has been measured for similar CdS NRs in organic solvent, prior to the exchange of the native phosphonate ligand by 11-MUA, to occur with a half-life of ~67 ns.[61] Because $k_{HT} >> k_{CR1}$ and both processes are independent of Pt size, the hole transfer step can be assumed to be of near unity QE and Pt size independent. Further transfer of the CB electron to the Pt tip (with a Pt size dependent rate constant k_{ET}, Figure 3D) forms a charge separated state (L^+-CdS-Pt$^-$). This process occurs on the same time scale as hole transfer in CdS NRs with large Pt and becomes slower in NRs with small Pt (Figure 3D). Its competition with the charge recombination process in L^+-CdS$^-$-Pt ($1/k_{CR2}$~57 ns, Figure 3D) determines the Pt size dependent ET QE (QE_{ET}). Further removal of the hole in the surface ligand to the solution

SD (L-cysteine) with a rate constant of k_{HS}, forms a long-lived L-CdS-Pt$^-$ species; and its competition with the charge recombination in L$^+$-CdS-Pt$^-$ (k_{CR3}) determines the QE of this hole scavenging process (QE_{HS}). As discussed above, the direct experimental determination of k_{CR3} is not feasible due to the lack of associated spectroscopic signatures (Figure S5). TA measurements of CdS-Pt in organic solvent (Figure S6 and 7), corresponding to CdS$^+$-Pt$^-$, shows that charge recombination, with a half lifetime of ~2.3 μs, is independent of the Pt size. We assume that charge recombination in L$^+$-CdS-Pt$^-$, in which the hole resides in the surface ligand instead of a surface site in L-CdS$^+$-Pt$^-$, should also be independent of the Pt size. This is consistent with the previous finding that charge recombination is determined by the slow rate of hole diffusion on the NR and is likely not sensitive to the Pt size dependent hole transfer step at the Pt/CdS interface.[59] Finally, in the water reduction stage, a proton or water is first reduced on L-CdS-Pt$^-$ to form L-CdS-Pt-H. This species can absorb another photon to repeat the process above to produce another Pt-H on the Pt particle and the two adsorbed H atoms diffuse together to form H_2. Alternatively, two L-CdS-Pt-H can find each other in solution to produce H_2. These processes (with a rate limiting rate constant k_{WR}) compete with charge recombination and gives rise a Pt size dependent water reduction QE (QE_{WR}). The light driven H_2 generation QE is the product of the QEs of these elementary stages according to Eq. (1).

$$QE_{H2} = QE_{HT} * QE_{ET}(d) * QE_{HS} * QE_{WR}(d) = C * QE_{ET}(d) * QE_{WR}(d) \qquad (1)$$

In Eq. (1) we have grouped the product of the size independent terms into a constant C ($= QE_{HT} * QE_{HS}$). In this simplified kinetic model, we have assumed that the rates of these elementary steps are distinctly different and can be modelled by the sequential kinetics scheme described above. This assumption is justified based on known time constants. For example, the hole transfer from trap states in CdS to the surface ligand L, occurring on the 100 ps time scale, [39, 51] is well separated from the next hole transfer event from the oxidized ligand to sacrificial donors in solution on the >> ns time scale. Similarly, while the initial electron transfer from the CdS to Pt is ultrafast (< 1ns time), the reduction of water on Pt and the H_2 evolution processes occurs on the much slower (~1.3 ms, SI2.2) time scale. Thus, it is also informative to divide the overall process into a charge separation stage (with a quantum efficiency of $QE_{CS} = QE_{HT} * QE_{ET}(d) * QE_{HS}$) and a water reduction stage (with a quantum efficiency of QE_{WR}), as shown

in Scheme 1B.

The QE_{ET} of different samples can be determined from transient absorption kinetics (Figure 3D) according to eq. (2).[62]

$$QE_{ET} = 1 + \int_0^\infty dt \frac{dS_{CdS}(t)}{dt} \frac{S_{CdS-Pt}(t)}{S_{CdS}(t)} \quad (2)$$

In eq. (2), $S_{CdS}(t)$ and $S_{CdS-Pt}(t)$ represents the time dependent probability distribution of the CdS conduction band electron in CdS and CdS-Pt NRs, respectively, which can be obtained from their 1Σ exciton bleach recovery kinetics. The calculated QE_{ET} values for CdS-Pt of different Pt sizes are shown in Figure 2 (orange pentagon). From the measured QE_{ET} and QE_{H_2}, $C * QE_{WR}$ can also be calculated according to eq. (1), which is also plotted in Figure 2.

The result in Figure 2 shows that the observed increase of $QE_{H_2}$with Pt particle sizes results from the size dependence of QE_{ET} and QE_{WR}, both increasing with the Pt particle size. Over the size regime studied, QE_{ET} values are significantly higher than C^*QE_{WR}. For example, for $CdSPt_{3.0nm}$ the QE_{ET} is ~88%, while $C * QE_{WR} = QE_{HT} * QE_{HS} * QE_{WR}(d)$ is ~ 44%, leading to a QE_{H_2} efficiency of only 38.3±5.1%. As discussed above, QE_{HT}~ 1, because of much faster hole transfer rate compared to the trap exciton decay in CdS.[39, 51] Thus, the low overall light to hydrogen conversion efficiency in $CdSPt_{3.0nm}$ can be attributed to small $QE_{HS} * QE_{WR}(d) \sim 44\%$.

According to the simplified kinetic model (Scheme 1B) and Figure 2, the size dependent QE_{ET} can be attributed to the size-dependent ET rate from the CdS to Pt. The origin of this dependence will be further discussed below. Two factors affecting size-dependent QE_{WR} should be considered: (i) the size dependent water reduction rate, k_{WR}, and (ii) the size dependent recombination between the electrons (e^-) in Pt and with the hole in the oxidized SDs. The Pt size dependence of this charge recombination process is unclear. If it is assumed to be size independent, our result would suggest higher water reduction rates in larger Pt particles. It has been reported previously that decreasing the Pt size from 3 nm particles to single atoms causes an order of magnitude decrease in the rate of electrocatalytic reduction of water (k_{WR}), which has been attributed to the size dependent of H* absorption energy and its effect on the rate limiting Pt-H formation step.[15] It is possible that the dark electrocatalytic property of Pt size dependence is well encoded into the photoelectrochemical performance, playing an

important role in controlling the second stage of the overall photoinduced H_2 generation process (Scheme 1B).

Size dependent electron transfer from CdS to Pt

As shown in Figure 3D, ET rates decrease in CdS-Pt samples with smaller average Pt sizes. According to Figure S1, there is a broad distribution of Pt particle sizes in CdS-Pt samples. As shown in Figure S9, a normalized comparison of exciton bleach kinetics of samples of different Pt sizes shows that the slow components (10^4-10^6 ps) of all samples are the same as that of CdS NRs without Pt, indicating the presence of a subpopulation that is ET inactive. This ET inactive subpopulation increases in samples with a smaller average Pt tip size. The percentage of this subpopulation is larger than the percentage of untipped nanorods in each sample. For instance, in $CdSPt_{0.7nm}$, about 80% of decay comes from ET inactive nanorods, while only around 30% nanorods are not tipped with small Pt clusters (Table S2). As shown in Figure S10, the subpopulation of ET inactive nanorods is consistent with subpopulations of untipped nanorods and nanorods with Pt particles smaller than 1 nm. This indicates extreme slow ET into small Pt clusters, which cannot compete with the intrinsic exciton recombination in CdS NRs. Thus, the decay of XB in CdS-Pt can be attributed to the ET into Pt size >1 nm. To understand the kinetics of exciton bleach recovery in the CdS-Pt samples, a model that considers the Pt size distribution is applied to fit the kinetics in Figure 3D, as described in SI4. In this model, we assume ET to a precise Pt size follows a single exponential decay with a size-dependent rate. Weighted by the Pt size distribution, the measured kinetics of solution ensemble is an average result covering all different sizes showing in the solution. The best fit according to this model is shown in Figure 3D and the fitted size dependent ET times for Pt size >1 nm are shown in Figure 4. In the calculation, we have binned the Pt sizes within 0.5 nm into a data point, which is shown as the error bar of the diameter in Figure 4. The plot of the logarithm of the fitted electron transfer lifetime vs Pt diameter shows a linear dependence with a slope of -5.6±0.6, indicating that the electron transfer time scales with the diameter (d) of the Pt particle as $d^{-5.6}$.

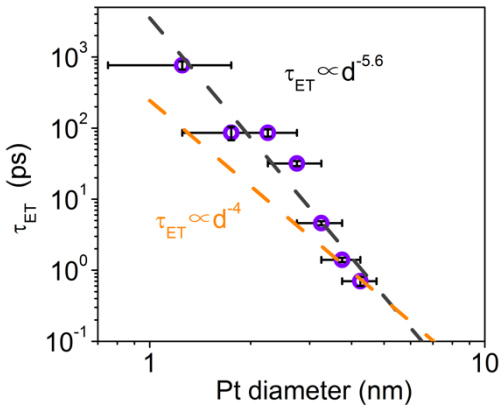

Figure 4. Pt size dependent electron transfer time. Estimated size-dependent electron transfer time obtained from the fit to the kinetics shown in Figure 3D. The plot of the logarithm of ET time vs the Pt size shows a linear dependence with a slope -5.6±0.6, indicating $\tau_{ET} \propto d^{-5.6}$ Also shown is the expected $\tau_{ET} \propto d^{-4}$ dependence according to the model described by Eq.(3). The error bar in the Pt diameter represents the bin size used in the fitting model.

The model for describing electron transfer from the CdS nanorod to the Pt tip remains unclear. This process can involve direct one-step tunneling of the electron from the trapped exciton state to the Pt. Alternatively, it can involve indirect activated diffusion process that consists of several steps: (i) Due to the columbic interaction between the electron and hole, to move freely, the electron firstly needs to be separated from the hole by thermal activation, (ii) diffusive transport of the electron to the CdS/Pt interface in the CdS, (iii) finally, the electron transfer across the CdS/Pt interface. The five CdS-Pt samples are prepared using the same CdS rod, which suggest they should have the same rates for the first and second steps. Thus, only the last step depends on the size of the Pt and varies in these samples. Within the activated diffusion model, the observation of the $d^{-5.6}$ dependence of the ET time (Figure 3D and 4) suggest that the ET rate is limited by the interfacial transfer step. Thus, in both models, the effective interfacial electron transfer rate can be described by the Fermi's golden rule as shown in eq. 3:[63]

$$k_{ET} = \frac{2\pi}{\hbar}\rho(E)|H(E)|^2 \quad (3)$$

$\rho(E)$ represents the density of states in the metal acceptors and can be expressed as $\rho(E) = V\frac{(2m_e^*)^{3/2}}{2\pi\hbar^3}\sqrt{E} \propto d^3\sqrt{E}$, with E being the energy difference between the CdS conduction band edge and the Pt sp band bottom. For large Pt particles, the CB states in Pt is continuous and E is nearly size-independent, which suggests that $\rho(E)$ scales with d^3. $|H(E)|^2$ is the modular square of the transition matrix from the initial state in the CdS CB to the final state in Pt. Within the tight binding model, the coupling strength is determined by the first layer of Pt atoms that are in contact with the CdS. Thus, $H(E)$ should be proportional to the number of Pt atoms at the interface, which scales with d^2, and the contribution of each interfacial Pt atom to a k state within the Pt, which scales with $1/\sqrt{N} \sim 1/\sqrt{d^3}$. These factors combine to lead to $|H(E)|^2 \sim d$. According to eq. (3), ET rate from the CdS to Pt should scale with d^4, or $\tau_{ET} \sim d^{-4}$, which is close to experimentally observed size dependence shown in Figure 4. Such steep dependence of ET rates on Pt diameter is consistent with the lack of ET activity in NRs with small Pt clusters. Previously, $|H(E)|^2$ for ET from the CdS rod to the Au tip is assumed to be independent of the Pt size.[36] This assumption is likely more valid when the size of the Pt exceeds the diameter of the CdS NRs and the contact area become independent of the Pt size. It should also be noted that the d^{-4} dependence is based on the assumption of continuous density of states in the Pt, which is likely not applicable for small Pt clusters with discrete conduction band states.

Photocatalytical H_2 production reactivities of other metal-tipped NRs have been reported previously. The H_2 production rate of CdS-Au NRs was reported to increase with gold diameters from 1.5±0.2 to 3.0±0.5 nm, followed by a decrease with Au sizes from 4.8±0.7 nm to 6.2±0.8 nm.[36] A similar trend was also reported in CdS-Ni NRs, in which an optimal diameter of Ni tip at around 5.2 nm was observed within a range of 2.3 nm to 10.1 nm.[37] Our trend of increasing H_2 production quantum efficiencies with the Pt size shown in Figure 2 is consistent with these previous reports in the small diameter range (<5 nm). The trend of size-dependent H_2 evolution performance of CdS-Pt at larger sizes can be predicted based on the above discussion of the size-dependent electron transfer and water reduction efficiencies. With increasing Pt size, electron transfer rate is assumed to increase rapidly with size, roughly scaling with $d^{5.6}$, and QE_{ET} increases with size until it saturates at nearly 100%; The electrocatalytic water reduction rate on Pt nanoparticles has been reported to increase with the Pt size until it

saturates at *d*~10 nm, which predicts a similar trend of QE_{WR}. As a result, QE_{H2} for CdS-Pt is predicted to increase with the Pt size until reaching a plateau value at larger size. This predicted trend does not agree with previous reported trends in CdS-Ni and CdS-Au NRs, [36-37] which show a decrease of QE_{H2} with the particle size beyond the optimal size. The origin of this disagreement is not clear. It is possible that size dependence of the catalytic H_2 reduction rates in Ni and Au metal nanoparticles are different from Pt. The predicted increase of CdS-to-Pt ET rate at larger Pt size is consistent with the observed trend in CdS-Au nanorods, but a decrease of ET rate beyond the optimal Ni particle size was observed in CdS-Ni NRs. The simple model described above does not account for any changes of the nature of CdS-Pt interface. Future direct experimental studies at larger Pt size are needed to fully investigate the size dependence beyond the small size regime studied in this work.

***Operando* electron transfer kinetics under CW illumination**

Under the CW illumination conditions of the light-driven H_2 generation measurement

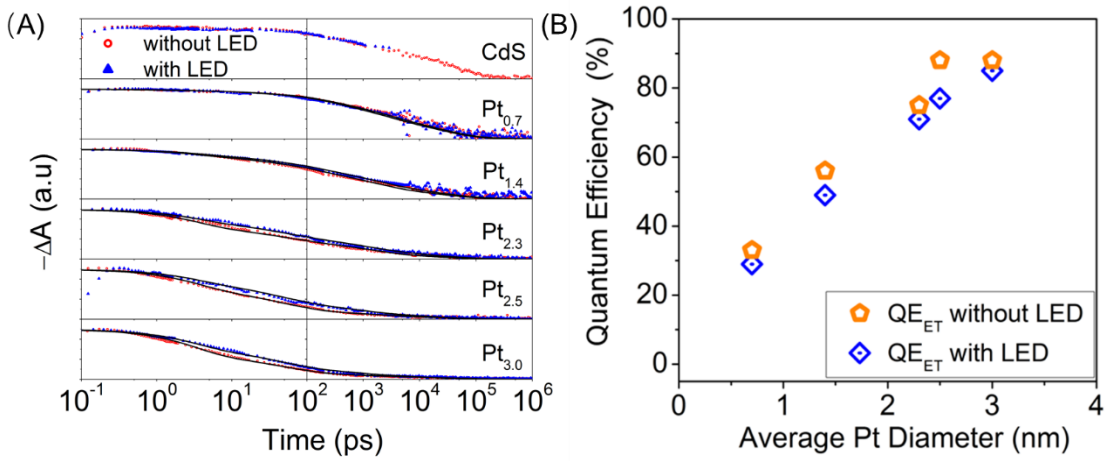

shown in Figure 2, each NR is estimated to absorb a photon in every 0.4 ms and generate a H_2 molecule in every 1.3 ms (see SI2.2 for details). Because of the relative slow H_2 evolution rate compared to excitation rate under TA measurement conditions, there may be accumulation of electrons in the Pt. To examine its effect of charge separation kinetics, we also carried out TA studies with the sample under the same CW illumination conditions used for the H_2 production measurement (SI3.4). TA spectra of CdS and CdS-Pt NRs samples with (Figure S8) and without (Figure 3A-C) CW illumination are similar. The XB bleach of untipped CdS NRs under CW illumination show identical decays as those measured under dark situations (Figure 4A, first panel,) which is consistent with faster electron-hole recombination (~57 ns) compared to photon absorption rate (~0.4 ms). Interestingly, for all CdS-Pt samples, the CdS XB decay become slower in the presence of CW illumination (Table S3), indicative of a slower ET rate. However, because ET lifetimes are still much faster than the intrinsic decay of exciton, the ET efficiencies of CdS-Pt under illumination, calculated using the method to be described below, is only lower by 5-10% than under dark conditions (Figure 4B). Such effect does not affect the qualitative understanding of the efficiency limiting factors of the hybrid photocatalyst above.

Figure 4. (A) Comparison of electron transfer kinetics (XB recovery kinetics) measured by TA spectroscopy in CdS and CdS-Pt samples with and without CW LED illumination at 405 nm. (B) Comparison of electron transfer quantum efficiency calcualted from the measured exciton bleach recovery kinetics of samples with and without LED illumination. The results in samples

without light illumination is from Figure 2C and 3D.

Key parameters for hybrid semiconductor/metal photocatalysts

Our findings provide important insight into designing photocatalysts that are based on semiconductor/metal catalyst hybrid materials. In general, both the quantum efficiencies for charge separation (including electron transfer, hole transfer, and hole scavenging) and catalytic reaction should be optimized to improve the quantum efficiency of overall light driven reactions. In CdS-Pt nanorods, increasing the average Pt size in the 1 - 4 nm size regime improves the catalyst performance by enhancing both the electron transfer of water reduction quantum efficiencies. In recent years, single atom or small cluster catalysis have received intense interest because of their high catalytic activity and cost-effectiveness. Our result shows that in CdS-Pt nanorods, the rate of electron transfer into <1 nm Pt cluster is too slow to compete with the electron-hole recombination due to the steep decrease of the electron transfer rate with the particles size ($d^{-5.6}$). Thus, significant challenges remain in designing efficient photocatalysts based on single atom or small cluster catalysts. First, the electron transfer rate into such small clusters should be improved. This can be done by shortening charge migration distance and increasing the interaction strength between metal and semiconductor support.[30] Second, the catalytical performance of small clusters on the semiconductor should be optimized, e.g. by changing the surface Pt^{2+}/Pt^0 ratio[25, 64], the surface indexes of Pt[65], and the surface ligands on Pt. Future work that focuses on improving the surface chemistry of small Pt clusters would be important for developing efficient photocatalytic systems with a catalyst loading approaching single atoms. Slowing down charge recombination processes through better design of nanostructures and coupling to faster oxidation processes will be essential to increasing the charge separation and water reduction efficiencies for smaller Pt clusters.

In photocatalyst design, it is important to consider the effects of size, number and weight percent of catalysts per absorber. In our CdS-Pt samples, most NRs contain only a single Pt tip, in which the catalyst weight percent scales the Pt size. Because balancing the cost of catalysts against the efficiency of catalysis is also an important design parameter, we have also estimated QE_{H_2} per unit Pt volume, i.e $QE_{H_2}/(\frac{4\pi}{3}r^3)$ with r being the Pt radius, as described in SI5. As

shown in Figure S11, the QE_{H_2}/volume values are ~3%/nm^3 for all samples, independent of the average Pt size. Also shown in Figure S11 is the calculated QE_{H_2}/volume values for previously reported CdS-Ni and CdS-Au NRs,[36-37] which decrease monotonically with the average particle size, reflecting the decrease of QE_{H_2} at larger catalyst particle size. It is unclear whether similar decrease will also be observed in CdS-Pt NRs with larger Pt tips. As shown in Table S2, with the increase of the average Pt size, the percentage of CdS-Pt NRs with two Pt tips increases. Previous studies of Pt decorated CdSe@CdS nanorods have reported that the H_2 production efficiency decrease with the number of Pt particles per NR.[47, 66] It has been attributed to the decreased probability of generating two Pt-H at the same Pt particle, which reduces the H_2 generation rate. In our samples, the H_2 generation QE increases at larger average Pt sizes, despite the increase of the percentage of NRs with two Pt tips, which may suggest that the QE increase due to larger size outcompetes the negative impact of having more rods with two tips. Our analyses above have focused on the effect the Pt particle size. It is unclear how the morphology (geometry) and exposed facets in the Pt tips change with the Pt size, which could have also important impacts on their performance.[65, 67] Thus, developing chemistry to precisely control the Pt particle size, size distribution, and facets would be important in investigating those questions and improving the H_2 generation performance of CdS-Pt NRs.

Conclusion

We have investigated the mechanism by which the Pt particle size affects the photocatalytic light-to-H_2 conversion efficiency of CdS-Pt nanorod heterostructures, a model system for hybrid semiconductor/metal photocatalysts. We observed that the light-to-H_2 conversion efficiency QE_{H2} increases from 0.5±0.2% to 38.3±5.1% when the average Pt particle size increases from 0.7±0.3 to 3.0 ±0.8 nm. The light-to-H_2 generation process involves multiple elementary forward (electron transfer, hole transfer, hole scavenging and proton reduction) and backward charge recombination steps, and their competitions determines the quantum efficiencies of the elementary steps and overall process. We propose a simplified kinetic model in which the overall light driven H_2 generation quantum efficiency is the product of the quantum efficiencies of four key steps: $QE_{H2} = QE_{HT} * QE_{ET}(d) * QE_{HS} * QE_{WR}(d)$.

To gain insight into the key Pt size dependent steps, we carried out *in situ* transient absorption measurement of charge separation of these nanorods under the same conditions as H_2 generation measurements. Both the rate and quantum efficiency of electron transfer from the CdS to Pt increase with the average Pt particle size. Our analysis suggests that QE_{ET} increases from 33% to 88% and the quantum efficiency of the remaining steps $C * QE_{WR}(d)$ increases from 2% to 44% when the average Pt particle size increases from 0.7±0.3 to 3.0 ±0.8 nm. The latter change is caused by the size dependence of $QE_{WR}(d)$ because C=$QE_{HT} * QE_{HS}$ is independent on the Pt size. The increase in the former can be attributed to faster electron transfer in larger Pt particle sizes and the increase in the latter may reflect faster water reduction rates in larger Pt particles. The increases of both electron transfer and water reduction quantum efficiencies account for the observed increase of overall light-to-H_2 generation quantum efficiency in nanorods with larger Pt sizes. Detailed analyses of electron transfer kinetics that account for the Pt tip size distribution reveal that the ET rate increases with the Pt diameter according to $d^{5.6\pm0.6}$ and reflect the size dependences of the electronic coupling strength between the CdS and Pt and the density of ET accepting states in Pt.

Our findings suggest that efficient hybrid semiconductor/metal photocatalysts require both efficient light driven charge separation from the semiconductor to the metal and fast catalysts to reduce the charge recombination loss. The observed steep decrease of interfacial charge transfer rate from the CdS to Pt at small particle sizes suggests significant challenges in designing efficient photocatalysts based on single atom or small cluster catalysts. In addition to increasing the catalytic rate of small clusters, efficient photocatalysts also require schemes to enhance forward electron and hole transfer rates and suppress multiple charge recombination processes in the overall photocatalytic system.

Supporting Information

Synthesis procedure, TEM images, Pt-tip size distribution, photocatalytical H_2 production measurements, transient absorption measurements, kinetics model and kinetics fitting details.

Acknowledgement

This material is based upon work supported by the U.S. Department of Energy, Office of Science, Office of Basic Energy Sciences, Solar Photochemistry Program under Award Number (DE-SC0008798). The transmission electron microscope images were taken at the

Robert P. Apkarian Integrated Electron Microscopy Core (IEMC) at Emory University. Scanning transmission electron microscopy was conducted at the Center for Nanophase Materials Sciences, which is a DOE Office of Science User Facility. Q. Zhao thanks the China Scholarship Council (CSC).

References:

1. Gust, D.; Moore, T. A.; Moore, A. L., Solar Fuels Via Artificial Photosynthesis. *Acc. Chem. Res.* **2009**, *42*, 1890-1898.

2. Meyer, T. J., Chemical Approaches to Artificial Photosynthesis. *Acc. Chem. Res.* **1989**, *22*, 163-170.

3. Tachibana, Y.; Vayssieres, L.; Durrant, J. R., Artificial Photosynthesis for Solar Water-Splitting. *Nat. Photon.* **2012**, *6*, 511-518.

4. Kudo, A.; Miseki, Y., Heterogeneous Photocatalyst Materials for Water Splitting. *Chem. Soc. Rev.* **2009**, *38*, 253-278.

5. Kranz, C.; Wachtler, M., Characterizing Photocatalysts for Water Splitting: From Atoms to Bulk and from Slow to Ultrafast Processes. *Chem. Soc. Rev.* **2021**, *50*, 1407-1437.

6. Wu, K.; Lian, T., Quantum Confined Colloidal Nanorod Heterostructures for Solar-to-Fuel Conversion. *Chem. Soc. Rev.* **2016**, *45*, 3781-810.

7. Maeda, K.; Domen, K., Photocatalytic Water Splitting: Recent Progress and Future Challenges. *J. Phys. Chem. Lett.* **2010**, *1*, 2655-2661.

8. Li, X.-B.; Tung, C.-H.; Wu, L.-Z., Semiconducting Quantum Dots For artificial Photosynthesis. *Nature Reviews Chemistry* **2018**, *2*, 160-173.

9. Li, X. B.; Xin, Z. K.; Xia, S. G.; Gao, X. Y.; Tung, C. H.; Wu, L. Z., Semiconductor Nanocrystals for Small Molecule Activation Via Artificial Photosynthesis. *Chem Soc Rev*

2020, *49*, 9028-9056.

10. Cheng, L.; Xiang, Q.; Liao, Y.; Zhang, H., Cds-Based Photocatalysts. *Energy & Environmental Science* **2018**, *11*, 1362-1391.

11. Somers, R. C.; Bawendi, M. G.; Nocera, D. G., Cdse Nanocrystal Based Chem-/Bio-Sensors. *Chem Soc Rev* **2007**, *36*, 579-91.

12. Roduner, E., Size Matters: Why Nanomaterials Are Different. *Chem. Soc. Rev.* **2006**, *35*, 583-592.

13. Zou, X.; Zhang, Y., Noble Metal-Free Hydrogen Evolution Catalysts for Water Splitting. *Chem. Soc. Rev.* **2015**, *44*, 5148-5180.

14. Cheng, N., et al., Platinum Single-Atom and Cluster Catalysis of the Hydrogen Evolution Reaction. *Nat. Commun.* **2016**, *7*, 13638.

15. Zhou, M.; Bao, S.; Bard, A. J., Probing Size and Substrate Effects on the Hydrogen Evolution Reaction by Single Isolated Pt Atoms, Atomic Clusters, and Nanoparticles. *J. Am. Chem. Soc.* **2019**, *141*, 7327-7332.

16. Cao, S.; Tao, F. F.; Tang, Y.; Li, Y.; Yu, J., Size- and Shape-Dependent Catalytic Performances of Oxidation and Reduction Reactions on Nanocatalysts. *Chem. Soc. Rev.* **2016**, *45*, 4747-4765.

17. Zheng, Y.; Jiao, Y.; Jaroniec, M.; Qiao, S. Z., Advancing the Electrochemistry of the Hydrogen-Evolution Reaction through Combining Experiment and Theory. *Angew. Chem. Int. Ed.* **2015**, *54*, 52-65.

18. Quinson, J., et al., Investigating Particle Size Effects in Catalysis by Applying a Size-Controlled and Surfactant-Free Synthesis of Colloidal Nanoparticles in Alkaline Ethylene

Glycol: Case Study of the Oxygen Reduction Reaction on Pt. *ACS Catal.* **2018**, *8*, 6627-6635.

19. Zhu, J.; Yang, M.-L.; Yu, Y.; Zhu, Y.-A.; Sui, Z.-J.; Zhou, X.-G.; Holmen, A.; Chen, D., Size-Dependent Reaction Mechanism and Kinetics for Propane Dehydrogenation over Pt Catalysts. *ACS Catal.* **2015**, *5*, 6310-6319.

20. Schweinberger, F. F., et al., Cluster Size Effects in the Photocatalytic Hydrogen Evolution Reaction. *J. Am. Chem. Soc.* **2013**, *135*, 13262-13265.

21. Karakus, M.; Sung, Y.; Wang, H. I.; Mics, Z.; Char, K.; Bonn, M.; Cánovas, E., Correlating Carrier Dynamics and Photocatalytic Hydrogen Generation in Pt Decorated Cdse Tetrapods as a Function of Cocatalyst Size. *J. Phys. Chem. C* **2017**, *121*, 13070-13077.

22. Imaoka, T.; Akanuma, Y.; Haruta, N.; Tsuchiya, S.; Ishihara, K.; Okayasu, T.; Chun, W. J.; Takahashi, M.; Yamamoto, K., Platinum Clusters with Precise Numbers of Atoms for Preparative-Scale Catalysis. *Nat. Commun.* **2017**, *8*, 688.

23. Dong, C.; Lian, C.; Hu, S.; Deng, Z.; Gong, J.; Li, M.; Liu, H.; Xing, M.; Zhang, J., Size-Dependent Activity and Selectivity of Carbon Dioxide Photocatalytic Reduction over Platinum Nanoparticles. *Nat. Commun.* **2018**, *9*, 1252.

24. Wei, Y.; Jiao, J.; Zhao, Z.; Zhong, W.; Li, J.; Liu, J.; Jiang, G.; Duan, A., 3d Ordered Macroporous Tio2-Supported Pt@Cds Core–Shell Nanoparticles: Design, Synthesis and Efficient Photocatalytic Conversion of Co2 with Water to Methane. *J. Mater. Chem. A* **2015**, *3*, 11074-11085.

25. Kim, G. J.; Kwon, D. W.; Hong, S. C., Effect of Pt Particle Size and Valence State on the Performance of Pt/Tio2 Catalysts for Co Oxidation at Room Temperature. *J. Phys. Chem. C* **2016**, *120*, 17996-18004.

26. Sung, Y.; Lim, J.; Koh, J. H.; Hill, L. J.; Min, B. K.; Pyun, J.; Char, K., Uniform Decoration of Pt Nanoparticles on Well-Defined Cdse Tetrapods and the Effect of Their Pt Cluster Size on Photocatalytic H2 Generation. *CrystEngComm* **2015**, *17*, 8423-8427.

27. Berr, M.; Vaneski, A.; Susha, A. S.; Rodríguez-Fernández, J.; Döblinger, M.; Jäckel, F.; Rogach, A. L.; Feldmann, J., Colloidal Cds Nanorods Decorated with Subnanometer Sized Pt Clusters for Photocatalytic Hydrogen Generation. *Appl. Phys. Lett.* **2010**, *97*, 093108.

28. Crampton, A. S.; Rotzer, M. D.; Ridge, C. J.; Schweinberger, F. F.; Heiz, U.; Yoon, B.; Landman, U., Structure Sensitivity in the Nonscalable Regime Explored Via Catalysed Ethylene Hydrogenation on Supported Platinum Nanoclusters. *Nat Commun* **2016**, *7*, 10389.

29. Li, X.; Bi, W.; Zhang, L.; Tao, S.; Chu, W.; Zhang, Q.; Luo, Y.; Wu, C.; Xie, Y., Single-Atom Pt as Co-Catalyst for Enhanced Photocatalytic H2 Evolution. *Adv. Mater.* **2016**, *28*, 2427-2431.

30. Gao, C.; Low, J.; Long, R.; Kong, T.; Zhu, J.; Xiong, Y., Heterogeneous Single-Atom Photocatalysts: Fundamentals and Applications. *Chem. Rev.* **2020**, *120*, 12175-12216.

31. Liu, L.; Corma, A., Metal Catalysts for Heterogeneous Catalysis: From Single Atoms to Nanoclusters and Nanoparticles. *Chem. Rev.* **2018**, *118*, 4981-5079.

32. Carbone, L.; Kudera, S.; Giannini, C.; Ciccarella, G.; Cingolani, R.; Cozzoli, P. D.; Manna, L., Selective Reactions on the Tips of Colloidal Semiconductor Nanorods. *J. Mater. Chem.* **2006**, *16*, 3952-3956.

33. Schlicke, H.; Ghosh, D.; Fong, L. K.; Xin, H. L.; Zheng, H.; Alivisatos, A. P., Selective Placement of Faceted Metal Tips on Semiconductor Nanorods. *Angew. Chem. Int. Ed.* **2013**, *52*, 980-982.

34. Habas, S. E.; Yang, P.; Mokari, T., Selective Growth of Metal and Binary Metal Tips on Cds Nanorods. *J. Am. Chem. Soc.* **2008**, *130*, 3294-3295.

35. Wächtler, M.; Kalisman, P.; Amirav, L., Charge-Transfer Dynamics in Nanorod Photocatalysts with Bimetallic Metal Tips. *J. Phys. Chem. C* **2016**, *120*, 24491-24497.

36. Ben-Shahar, Y.; Scotognella, F.; Kriegel, I.; Moretti, L.; Cerullo, G.; Rabani, E.; Banin, U., Optimal Metal Domain Size for Photocatalysis with Hybrid Semiconductor-Metal Nanorods. *Nat. Commun.* **2016**, *7*, 10413.

37. Nakibli, Y.; Mazal, Y.; Dubi, Y.; Wachtler, M.; Amirav, L., Size Matters: Cocatalyst Size Effect on Charge Transfer and Photocatalytic Activity. *Nano Lett.* **2018**, *18*, 357-364.

38. Ben-Shahar, Y.; Philbin, J. P.; Scotognella, F.; Ganzer, L.; Cerullo, G.; Rabani, E.; Banin, U., Charge Carrier Dynamics in Photocatalytic Hybrid Semiconductor-Metal Nanorods: Crossover from Auger Recombination to Charge Transfer. *Nano Lett.* **2018**, *18*, 5211-5216.

39. Li, Q.; Zhao, F.; Qu, C.; Shang, Q.; Xu, Z.; Yu, L.; McBride, J. R.; Lian, T., Two-Dimensional Morphology Enhances Light-Driven H2 Generation Efficiency in Cds Nanoplatelet-Pt Heterostructures. *J. Am. Chem. Soc.* **2018**, *140*, 11726-11734.

40. Amirav, L.; Alivisatos, A. P., Photocatalytic Hydrogen Production with Tunable Nanorod Heterostructures. *J. Phys. Chem. Lett.* **2010**, *1*, 1051-1054.

41. Vamvasakis, I.; Liu, B.; Armatas, G. S., Size Effects of Platinum Nanoparticles in the Photocatalytic Hydrogen Production over 3d Mesoporous Networks of Cds and Pt Nanojunctions. *Advanced Functional Materials* **2016**, *26*, 8062-8071.

42. Wu, K.; Zhu, H.; Liu, Z.; Rodriguez-Cordoba, W.; Lian, T., Ultrafast Charge Separation and Long-Lived Charge Separated State in Photocatalytic Cds-Pt Nanorod

Heterostructures. *J. Am. Chem. Soc.* **2012**, *134*, 10337-10340.

43. Shabaev, A.; Efros, A. L., 1d Exciton Spectroscopy of Semiconductor Nanorods. *Nano Lett.* **2004**, *4*, 1821-1825.

44. Efros, A. L.; Rosen, M., The Electronic Structure of Semiconductor Nanocrystals. *Annu. Rev. Mater. Sci.* **2000**, *30*, 475-521.

45. Henglein, A.; Ershov, B. G.; Malow, M., Absorption Spectrum and Some Chemical Reactions of Colloidal Platinum in Aqueous Solution. *J. Phys. Chem.* **1995**, *99*, 14129-14136.

46. Sakimoto, K. K.; Wong, A. B.; Yang, P., Self-Photosensitization of Nonphotosynthetic Bacteria for Solar-to-Chemical Production. *Science* **2016**, *351*, 74-77.

47. Kalisman, P.; Nakibli, Y.; Amirav, L., Perfect Photon-to-Hydrogen Conversion Efficiency. *Nano Lett.* **2016**, *16*, 1776-1781.

48. Simon, T., et al., Redox Shuttle Mechanism Enhances Photocatalytic H2 Generation on Ni-Decorated Cds Nanorods. *Nat. Mater.* **2014**, *13*, 1013-1018.

49. Zhao, F.; Li, Q.; Han, K.; Lian, T., Mechanism of Efficient Viologen Radical Generation by Ultrafast Electron Transfer from Cds Quantum Dots. *The Journal of Physical Chemistry C* **2018**, *122*, 17136-17142.

50. Zhu, H.; Song, N.; Lv, H.; Hill, C. L.; Lian, T., Near Unity Quantum Yield of Light-Driven Redox Mediator Reduction and Efficient H2 Generation Using Colloidal Nanorod Heterostructures. *J Am Chem Soc* **2012**, *134*, 11701-8.

51. Wu, K.; Chen, Z.; Lv, H.; Zhu, H.; Hill, C. L.; Lian, T., Hole Removal Rate Limits Photodriven H2 Generation Efficiency in Cds-Pt and Cdse/Cds-Pt Semiconductor Nanorod-Metal Tip Heterostructures. *J. Am. Chem. Soc.* **2014**, *136*, 7708-7716.

52. Yang, W., et al., Surface-Ligand “Liquid” to “Crystalline” Phase Transition Modulates the Solar H2 Production Quantum Efficiency of Cds Nanorod/Mediator/Hydrogenase Assemblies. *ACS Appl. Mater. Interfaces* **2020**, *12*, 35614-35625.

53. Li, X. B.; Li, Z. J.; Gao, Y. J.; Meng, Q. Y.; Yu, S.; Weiss, R. G.; Tung, C. H.; Wu, L. Z., Mechanistic Insights into the Interface-Directed Transformation of Thiols into Disulfides and Molecular Hydrogen by Visible-Light Irradiation of Quantum Dots. *Angew Chem Int Ed Engl* **2014**, *53*, 2085-9.

54. Zhu, H.; Song, N.; Rodriguez-Cordoba, W.; Lian, T., Wave Function Engineering for Efficient Extraction of up to Nineteen Electrons from One Cdse/Cds Quasi-Type Ii Quantum Dot. *J. Am. Chem. Soc.* **2012**, *134*, 4250-4257.

55. Zhu, H.; Lian, T., Wavefunction Engineering in Quantum Confined Semiconductor Nanoheterostructures for Efficient Charge Separation and Solar Energy Conversion. *Energy Environ. Sci.* **2012**, *5*, 9406-9418.

56. Liu, Y.; Cullen, D. A.; Lian, T., Slow Auger Recombination of Trapped Excitons Enables Efficient Multiple Electron Transfer in Cds-Pt Nanorod Heterostructures. *J. Am. Chem. Soc.* **2021**, *143*, 20264-20273.

57. Berr, M. J.; Vaneski, A.; Mauser, C.; Fischbach, S.; Susha, A. S.; Rogach, A. L.; Jackel, F.; Feldmann, J., Delayed Photoelectron Transfer in Pt-Decorated Cds Nanorods under Hydrogen Generation Conditions. *Small* **2012**, *8*, 291-297.

58. Yang, W.; Godin, R.; Kasap, H.; Moss, B.; Dong, Y.; Hillman, S. A. J.; Steier, L.; Reisner, E.; Durrant, J. R., Electron Accumulation Induces Efficiency Bottleneck for Hydrogen Production in Carbon Nitride Photocatalysts. *J. Am. Chem. Soc.* **2019**, *141*, 11219-11229.

59. Utterback, J. K.; Grennell, A. N.; Wilker, M. B.; Pearce, O. M.; Eaves, J. D.; Dukovic, G., Observation of Trapped-Hole Diffusion on the Surfaces of Cds Nanorods. *Nat. Chem.* **2016**, *8*, 1061-1066.

60. Cline, R. P.; Utterback, J. K.; Strong, S. E.; Dukovic, G.; Eaves, J. D., On the Nature of Trapped-Hole States in Cds Nanocrystals and the Mechanism of Their Diffusion. *J. Phys. Chem. Lett.* **2018**, *9*, 3532-3537.

61. Wu, K.; Du, Y.; Tang, H.; Chen, Z.; Lian, T., Efficient Extraction of Trapped Holes from Colloidal Cds Nanorods. *J Am Chem Soc* **2015**, *137*, 10224-30.

62. Utterback, J. K.; Wilker, M. B.; Mulder, D. W.; King, P. W.; Eaves, J. D.; Dukovic, G., Quantum Efficiency of Charge Transfer Competing against Nonexponential Processes: The Case of Electron Transfer from Cds Nanorods to Hydrogenase. *J. Phys. Chem. C* **2018**, *123*, 886-896.

63. Canovas, E.; Moll, P.; Jensen, S. A.; Gao, Y.; Houtepen, A. J.; Siebbeles, L. D.; Kinge, S.; Bonn, M., Size-Dependent Electron Transfer from Pbse Quantum Dots to Sno2 Monitored by Picosecond Terahertz Spectroscopy. *Nano Lett.* **2011**, *11*, 5234-5239.

64. Wang, Y.; Wang, Y.; Xu, R., Photochemical Deposition of Pt on Cds for H2 Evolution from Water: Markedly Enhanced Activity by Controlling Pt Reduction Environment. *J. Phys. Chem. C* **2013**, *117*, 783-790.

65. Wang, H.; Gu, X.-K.; Zheng, X.; Pan, H.; Zhu, J.; Chen, S.; Cao, L.; Li, W.-X.; Lu, J., Disentangling the Size-Dependent Geometric and Electronic Effects of Palladium Nanocatalysts Beyond Selectivity. *Sci. Adv.* **2019**, *5*, eaat6413.

66. Nakibli, Y.; Kalisman, P.; Amirav, L., Less Is More: The Case of Metal Cocatalysts. *J*

Phys Chem Lett **2015**, *6*, 2265-2268.

67. Li, Z.; Ji, S.; Liu, Y.; Cao, X.; Tian, S.; Chen, Y.; Niu, Z.; Li, Y., Well-Defined Materials for Heterogeneous Catalysis: From Nanoparticles to Isolated Single-Atom Sites. *Chemical Reviews* **2020**, *120*, 623-682.
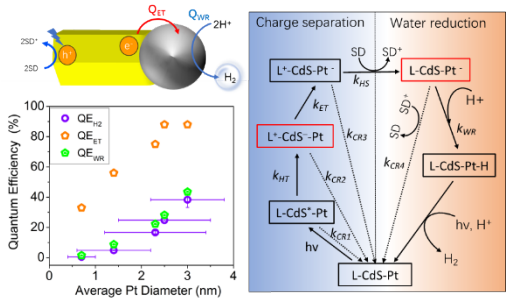
Table of Content Figure: